International Journal of Marine Science and Technology, vol. 2, no. 2, pp. 1–7, 2026
http://doi.org/10.65154/ijmst.55

e-ISSN: 3093-3609
https://i-jmst.vimaru.edu.vn

Numerical Investigation of Cavitation-induced Noise and Hydrodynamic Instability Around a Two-dimensional Hydrofoil

Minh Duc Nguyen, Ngoc Tu Tran, and Van Duyen Pham*

Abstract: In this numerical study, physical characteristics of cavitating flow around a two-dimensional hydrofoil was investigated using a Large Eddy Simulation (LES) framework. To capture the phase change, the Schnerr–Sauer cavitation model was applied to the simulation. First, the numerical results were carefully validated with current experimental study to ensure the accuracy of the numerical scheme. Then, systematic analysis of cavity evolution around the hydrofoil, velocity fields and streamline behaviors, and pressure distribution on the surface of the hydrofoil under two different flow conditions (σ = 2.57 and 4.95) were carried out. The results indicated that cavitation numbers have significant effects on the formation of the cavity as well as stability of the cavity dynamics. In particular, at high cavitation number, no cavity was observed on the suction side of the hydrofoil. However, as the cavitation number decreases to 2.57, the local pressure dropped significantly, leading to cavity formation. In addition, the acoustic analysis showed that cavitation substantially increased the sound pressure level (SPL) over a wide range of the frequencies. Moreover, formation of cavities on the suction side of the hydrofoil significantly induced instability of the hydrodynamic forces. Findings from this numerical study demonstrate unexpected influences of the cavitating flow on the hydrofoil. This provides valuable insight into the design and optimization of the hydrofoil geometry to reduce cavitation effects.

Keywords: Acoustics characteristics, cavitation, CFD, hydrodynamic forces, LES.

1. INTRODUCTION

For underwater vehicles, cavitation is serious phenomenon that occurs when the local pressure drops below the vapor pressure of the liquid. This leads to the formation of tiny bubbles. Due to the flow interaction, these bubbles move to the high-pressure region, then they collapse, causing the generation of the shock wave on the surface of the underwater system. This usually induces disadvantages for the vehicle such as vibration of the hydrodynamic forces, noise and surface erosion.

In current decades, numerous studies have been carried out to investigate physical characteristics of the cavitating flow by both tunnel test and numerical method [1–8]. In particular, Ahn et al. conducted an experiment to examine the coherent structure and acoustic feature induced by the cavitating flow around two-dimensional hydrofoil across various cavitation numbers and angles of attack [1]. The results showed that both angle of attack and cavitation number have significant effects on the formation of cavity. Using the high-speed camera, Ahn et al. successfully observed the cavitating behavior on the hydrofoil with coherent structure. In addition, the noise characteristic was investigated using pressure sensor. The results indicated that formation of the cavity induces higher sound pressure levels.

Simanto et al., Kadivar et al., and Zhang et al. further investigated effects of passive control system on the cavitating flow. In particular, applying the leading-edge protuberances, Simanto et al. [2] reported that changing the leading-edge of the hydrofoil with protuberances can cause significant reduction of cavity formation and noise characteristics. Kadivar et al. and Zhang et al. caried out experiments using cavitating bubble generation [3,4] to control unsteady cavitating flow. The results showed that the device can successfully control the re-entrant jet and cavitating shedding behavior.

Recent studies have shown that cavitating flow induces variation in the hydrodynamic forces and pressure distribution on the surface of the vehicle [5-7]. In particular, Heo et al. [5] conducted numerical simulations to investigate the noise characteristic

Manuscript received March 12, 2026; received in revised form April 06, 2026; accepted April 16, 2026; available online June 30, 2026.

Minh Duc Nguyen is with the Cat Tuong Nguyen - LA Company Limited, Long An, Vietnam (e-mail: duc82nguyen1011@gmail.com). Ngoc Tu Tran and Van Duyen Pham are the Faculty of Shipbuilding, Vietnam Maritime University, Haiphong, Vietnam (e-mails: tutn.dt@vimaru.edu.vn and duyenpv.vck@vimaru.edu.vn).
* Corresponding author.

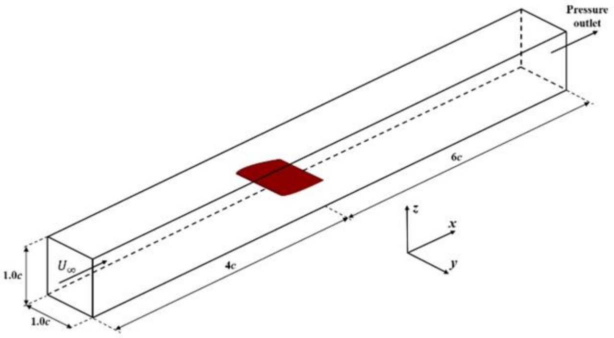

Fig. 1. Schematic of computational domain and boundaries conditions.

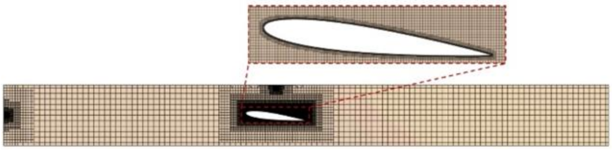

Fig. 2. Computational mesh.

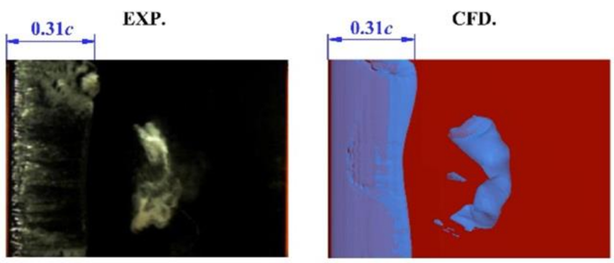

Fig. 3. Validation of numerical result against experiment by Simanto et al. [2] (α =7°, σ=2.57).

induced by cavitation. In this work, 7° angle of attack of two-dimensional hydrofoil was considered under various cavitation numbers (σ = 2.05, 2.27, and 2.53). The results showed that LES provides more consistent results with experiment compared to RANS simulation. In addition, the sound pressure level (SPL) increases with further reduction of the cavitation number. By another numerical work, Li et al. [6] reported that variations in the hydrodynamic performance are significantly influenced by formation of cavitation on the hydrofoil. In the latest study, Simanto et al. [7] carried out experiments to compare the flow characteristics in both cavitating and non-cavitating conditions using particle image velocimetry (PIV). The results showed that cavitation induces vortex structures and re-entrant jet formation, and then increasing the vortex shedding behavior. Although above-mentioned studies have reported significant characteristics of cavitating flow around the hydrofoil, systematical investigation of cavitating flow and its effects on the velocity distribution, flow streamlines and pressure behavior are insufficient. This requires deeper analysis and quantitative investigation.

In this study, we apply LES and the Schnerr–Sauer cavitation model to capture the cavitating flow around a two-dimensional hydrofoil. The advantages of the LES have been illustrated in our previously published works

Table 1. Mesh independent test for drag force coefficient.

No.	Mesh	Cells	C_D	GCI (%)	Error (%)
1	Coarse	3.2M	0.065		
2	Fine	9.0M	0.073	11.22	12.31
3	Very fine	25.2M	0.075	4.56	2.06

Table 2. Mesh independent test for lift force coefficient.

No.	Mesh	Cells	C_L	GCI (%)	Error (%)
1	Coarse	3.2M	0.86		
2	Fine	9.0M	0.992	13.99	15.35
3	Very fine	25.2M	0.998	1.34	0.61

[8-9]. After successful validation of the numerical scheme, we calculated two cavitation numbers (2.57 and 4.95). These conditions are selected following previous experiment reported by Simanto et al. [2]. By this work, effects of the cavitating flow on the velocity profile, turbulent coherent structure, acoustic features and pressure distribution are carefully analyzed.

2. NUMERICAL METHOD

In this study, large-eddy simulation approach (LES) is adopted to solve the governing equations. LES employs a spatial filtering operation to separate the larger-scale turbulent structures from the smaller ones. This filtering operation separates the flow into resolved (larger-scale) and sub-grid-scale (SGS) components [12]. By applying a filtering function, we obtained the LES continuity and momentum equations:

$$\frac{\partial \rho_m}{\partial t} + \frac{\partial}{\partial x_i}\left(\rho_m \bar{u}_i\right) = 0 \tag{1}$$

$$\begin{aligned}&\frac{\partial}{\partial t}\left(\rho_m \bar{u}_i\right) + \frac{\partial}{\partial x_j}\left(\rho_m \bar{u}_i \bar{u}_j\right) \\ &= -\frac{\partial \bar{P}}{\partial x_i} + \frac{\partial}{\partial x_j}\left(\mu_m \frac{\partial \bar{u}_i}{\partial x_j}\right) - \frac{\partial \tau_{ij}}{\partial x_j} + \rho_m g\end{aligned} \tag{2}$$

where $\bar{u}$ and $\bar{P}$ represent the filtered velocity and pressure field, and $\bar{\tau}_{ij}$ represents the sub-grid-scale (SGS) stresses. The sub-grid-scale (SGS) stresses is defined as

$$\bar{\tau}_{ij} = \rho_m\left(\overline{u_i u_j} - \bar{u}_i \bar{u}_j\right) \tag{3}$$

The SGS stress is modeled by the Smagorinsky-Lilly model where the local SGC stresses are taken to be proportional to the local strain rate tensor, $\bar{S}_{ij}$.

$$\begin{aligned}\bar{\tau}_{ij} &= -2\mu_{SGS}\bar{S}_{ij} + \frac{1}{3}\tau_{ij}\delta_{ij} \\ &= -\mu_{SGS}\left(\frac{\partial \bar{u}_i}{\partial x_j} + \frac{\partial \bar{u}_j}{\partial x_i}\right) + \frac{1}{3}\tau_{ij}\delta_{ij}\end{aligned} \tag{4}$$

where μ_{SGS} represents SGS viscosity, and it is

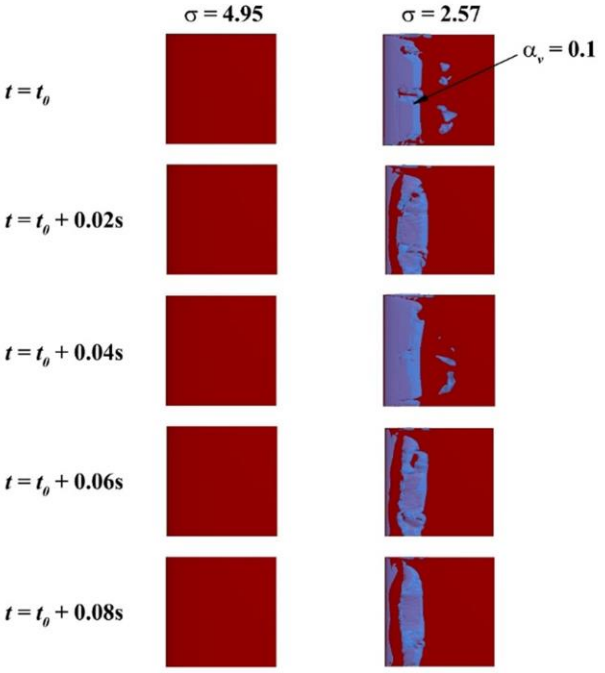

Fig. 4. Evolution of cavity under various cavitation numbers (top view).

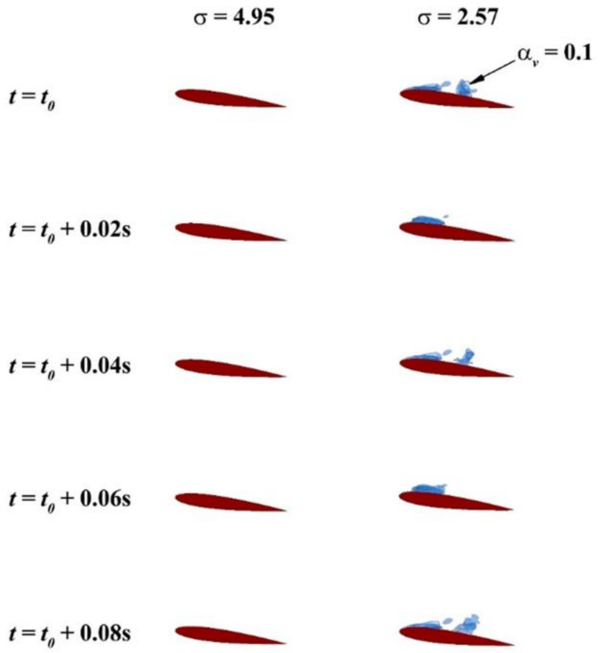

Fig. 5. Evolution of cavity under various cavitation numbers (side view).

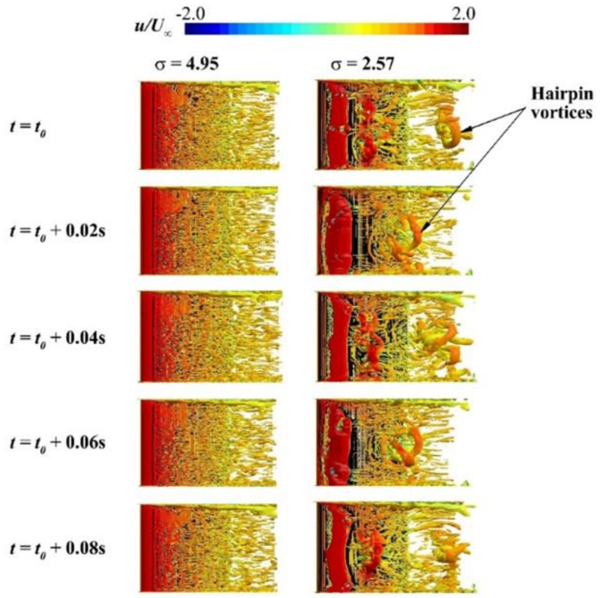

Fig. 6. Comparison of vortex structures on the suction side of the hydrofoil from the top view. The vortex structures are visualized and colored according to the streamwise velocity component.

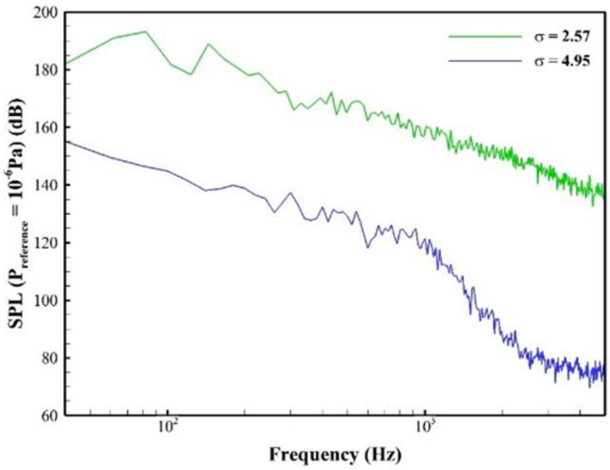

Fig. 7. Comparison of sound pressure level induced by non-cavitating and cavitating conditions.

evaluated by Eq. (5). In this equation, CSGS is constant and C_{SGS} = 0.1. Δ*s* is mixing length of the SGS model, and it is defined as Eq. (7) in which *V*, *K*, C_W represent the volume of a grid cell, the von Karman constant and a WALE model parameter, respectively. In this work, the WALE model parameter (C_W = 0.544) was chosen.

$$\mu_{SGS} = \rho\left(C_{SGS}\Delta_s\right)^2\left|\bar{S}\right| = \rho\left(C_{SGS}\Delta_s\right)^2\sqrt{2\bar{S}_{ij}\bar{S}_{ij}} \quad (5)$$

$$\bar{S}_{ij} = \frac{1}{2}\left(\frac{\partial\bar{u}_i}{\partial x_j} + \frac{\partial\bar{u}_j}{\partial x_i}\right) \quad (6)$$

$$\Delta_s = \min\left(\mathrm{K}_d, C_W V^{\frac{1}{3}}\right) \quad (7)$$

In the numerical calculation, the Schnerr–Sauer cavitation model [13] was applied to simulate the phase change from water to vapor. The governing equation for the vapor is as follows:

$$\frac{\partial\alpha_v}{\partial t} + \frac{\partial\left(\alpha_v u_i\right)}{\partial x_i} = \frac{1}{\rho_v}\left(\dot{m}^+ - \dot{m}^-\right) \quad (8)$$

$$\dot{m}^+ = \alpha_v\left(1-\alpha_v\right)\frac{\rho_w\rho_v}{\rho_m}\frac{3}{R_b}\sqrt{\frac{2}{3}\frac{\left(p_v - p\right)}{\rho_w}}, \quad p \le p_v \quad (9)$$

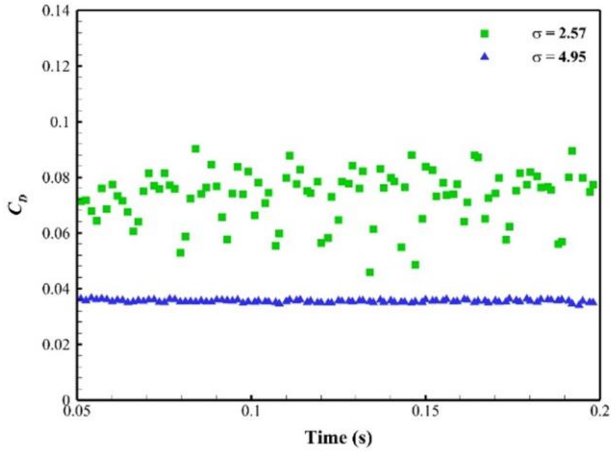

(a)

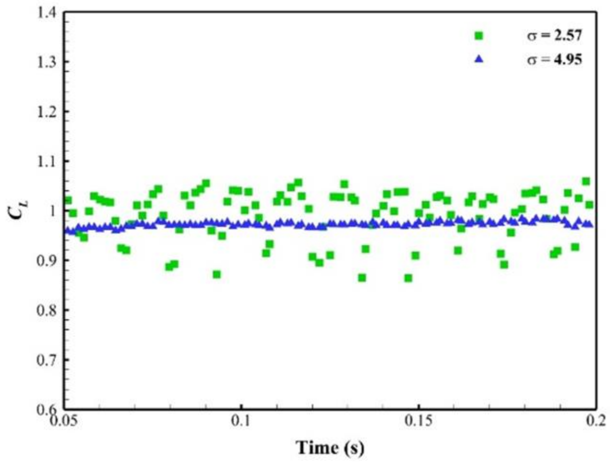

(b)

Fig. 8. Comparison of hydrodynamic forces acting on hydrofoil. (a) drag force coefficient, (b) lift force coefficient.

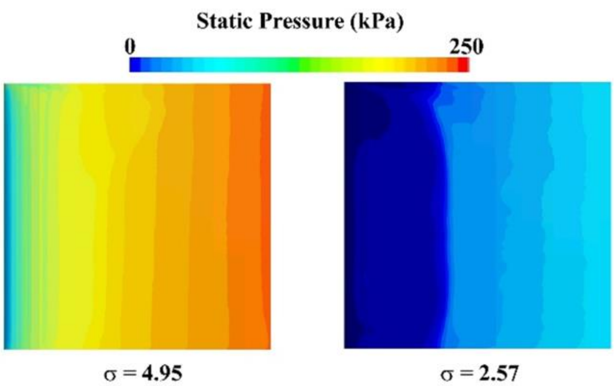

Fig. 9. Comparison of time-averaged pressure on suction side of the test model.

$$\dot{m}^- = \alpha_v \left(1-\alpha_v\right) \frac{\rho_w \rho_v}{\rho_m} \frac{3}{R_b} \sqrt{\frac{2}{3} \frac{\left(p-p_v\right)}{\rho_w}}, \; p \geq p_v \quad (10)$$

$$R_b = \left(\frac{\alpha_v}{1-\alpha_v} \frac{3}{4\pi} \frac{1}{N_b} \right)^{\frac{1}{3}} \quad (11)$$

where $\dot{m}^+$ and $\dot{m}^-$ are the mass transfer rates due to the evaporation and condensation, respectively. α_v, N_b and R_b are the volume fraction of the vapor, the nuclei density per volume of liquid water and the bubble diameter, respectively.

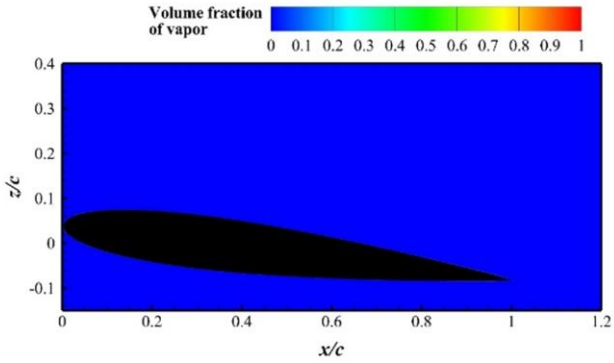

(a)

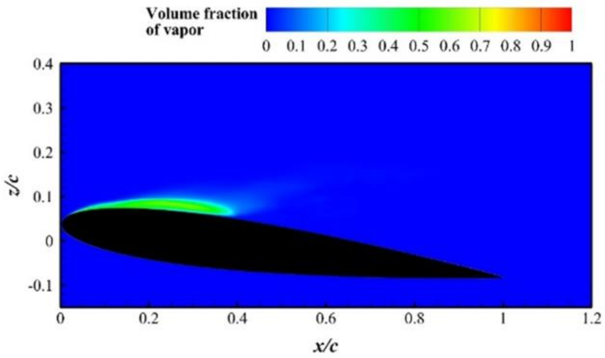

(b)

Fig. 10. Time-averaged volume fraction of vapor under various cavitation numbers. (a) σ=4.95, (b) σ=2.57.

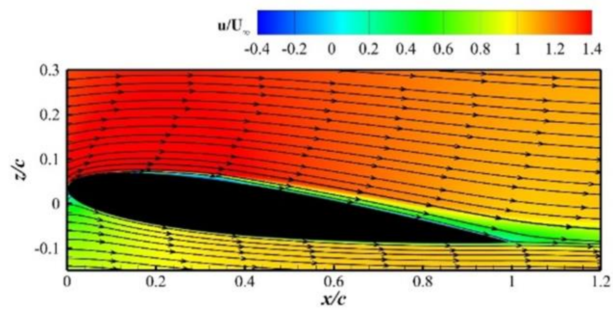

(a)

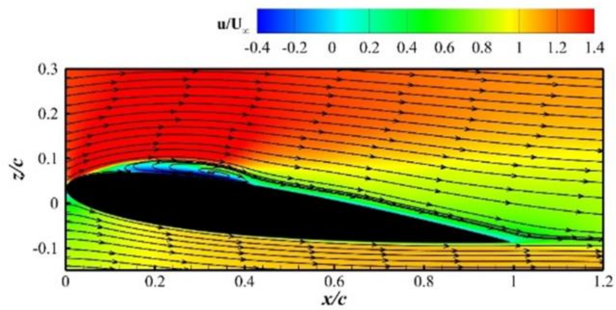

(b)

Fig. 11. Time-averaged streamlines around hydrofoil under various cavitation numbers. (a) σ=4.95, (b) σ=2.57.

As shown in Fig. 1, the schematic view of computational domain and boundary conditions are presented. In this work, a two-dimensional hydrofoil (NACA0012) with chord length (*c*) of 100 mm and span length (*s*) of 100 mm are considered. The domain is designed according to experiment conditions as reported by Simanto et al. [2]. In particular, the domain has a square section with dimensions of 100×100 mm. The distance between the inlet and outlet boundaries to the rotational point of the test model are 4*c* and 6*c*, respectively. For boundary conditions, the velocity inlet is applied for the inlet, whereas the outlet is considered to be pressure outlet. Free-stream velocity and pressure outlet are set to exact values in the experiment [2] to obtain similar cavitation numbers (2.57 and 4.95). In addition, the hydrofoil surface and computational walls are considered with no-slip wall. This allows similar flow conditions with experiment.

Figure 2 presents the computational mesh. In this work, we apply the mesh generation tool supported by STARCCM. The computational mesh is generated with fine mesh around the test model to capture detailed cavitating behavior. To examine the mesh independent test, three numbers of mesh are generated by changing the cell size. In particular, the coarse mesh, fine mesh and very fine mesh are created with cell numbers of 3.2M, 9.0M and 25.2M, respectively. As shown in Tables 1 and 2, Grid Convergence Index (GCI) for hydrodynamic forces are compared among three mesh [10]. The results show that the fine and very fine mesh have GCI of 4.56% and 1.34% for drag and lift coefficient, respectively. Whereas these indexes are 11.22% and 13.99% for the coarse mesh and fine mesh. This indicates that the fine and very fine mesh provides similar results. To receive balance between the computational cost and accuracy, the fine mesh is selected for all simulations.

The numerical scheme of LES framework and cavitation model has been carefully validated in our previous works [8,9]. To confirm the accuracy of the model, Fig. 3 compares the cavitation behavior between the current numerical result and experiment reported by Simanto et al. [2]. As shown in the figure, the numerical scheme successfully captures the cavitating flow including the cavity size and shedding behavior. In addition, as shown in Fig. 3, the cavity length of 0.31*c* is observed in both present simulation and experiment data, indicating a good agreement between the numerical simulation and experiment.

3. RESULTS AND DISCUSSION

In this section, effects of cavitating flow on the velocity distribution, the flow streamlines, turbulent coherent structure, pressure distribution and hydrodynamic performances are qualitatively and quantitatively investigated. To clearly visualize the cavitating flow and internal flow, the cavity is observed with 10% volume fraction of vapor and colored by blue with opacity of 50%. During the simulation, two cavitation numbers (2.57 and 4.95) are set to the flow condition. The hydrofoil is positioned at 7° angle of attack. In this study, cavitation numbers of 2.57 and 4.95 are strictly considered due to following reasons. First, as stated in the validation section, the numerical simulations are validated against the experiment data resported by Simanto et al. (2022). Therefore, for the purpose of the validation, these two cavitation numbers are selected. Secondly, under these cavitation numbers both cavitating and non-cavitating flow are examined to illustrate effects of cavitation on the noise characteristics and hydrodynamic performance. This provides good comparison of the physical characteristics of flow around the two-dimensional hydrofoil under effects of cavitating flow.

For cavitating flow, cavitation number is defined as $\sigma = (p_\infty - p_v)/\ (0.5\rho U_\infty^2)$, where p_∞ is free-stream ambient pressure, p_v is the vapor pressure, ρ is density of water, and U_∞ is free-stream velocity. In this study, cavitation numbers of 2.57 and 4.95 are strictly considered. Reduction of cavitation number is induced by decreasing of the free-stream ambient pressure (p_∞) under a constant free-stream velocity (U_∞). This leads to local pressure decreasing below the vapor pressure. As a consequence, cavitation forms and causes significant effects such as increasing the noise level and instability of hydrodynamic performance. Therefore, cavitation numbers have been considered as an important non-dimensional parameter to predict the cavitating flow.

Cavitating flow around the hydrofoil is influenced by several factors such as angle of attack, cavitation number, and dissoved air conditions. In this study, 7° angle of attack is considered under cavitation number of 2.57 and 4.95. As shown in the validation part, under flow condition of 7° angle of attack and cavitation number of 2.57, cavitation is clearly observed in both experiment and current simulation. Under these flow conditions, the local presure at the critical region (i.e. leading-edge) decreases below the vapor pressure of the water. As a result, cavitation occurs event at small angles of attack. In practical applications, this angle of attack is considered for high-speed lifting surfaces such as control hydrofoils of the high-speed vessels or rudder of high-speed supercavitating torpedoes.

Figures 4 and 5 present the evolution of the cavity with development of physical time from a top and side view perspective. As shown in the figures, at high cavitation number (σ = 4.95), no cavitation has been observed on the suction side of the hydrofoil. This indicates that local pressure remains above the vapor pressure of the water. However, as the cavitation number decreases to 2.57, cavitation occurs on the leading-edge of the hydrofoil, then cavitation moves to the down-stream of the hydrofoil with obvious shedding behavior. Obviously, the flow around the hydrofoil should satisfy the mass conservation. If the area decreases due to non-zero angles of attack, the velocity of the liquid particles should increase to maintain a constant volumetric flow rate of water passing the hydrofoil. As the velocity increases, according to Bernoulli's principle, the pressure will be decreased. At non-zero angles of attack, the leading edge of the hydrofoil plays as acceleration region. As a consequence, the cavitation will occur first near the leading edge, then it moves downstream and processes to shedding phenomenon. Corresponding to the physical time, the cavity forms and and collapse with certain frequencies. As the cavity collapses, smaller pockets of cavity are observed. This can lead to variations in the hydrodynamic forces and the noise signal. This will be investigated in detail.

As the cavity forms and collapses due to the high-pressure conditions, turbulent coherent structures can be influenced. To have deeper understanding of this phenomenon, turbulent structures of the flow are compared using Q-criterion ($Q = 10^5$ /s^2). As shown in Fig. 6, the Q-criterion is colored by streamwise velocity and normalized by free-stream velocity. As seen in the figure, at high cavitation number, number of small-scale turbulent structures are clearly observed. This indicates that characteristics of flow behavior such as the hydrodynamic forces are stable. In contrast, as cavitation numbers decrease to 2.57, small-scaled turbulent structures have been replaced with large-scale structures. Especially, Hairpin vortices are generated as the cavity collapses. The Hairpin vortex is mainly formed in the shear flow that combines with vortex stretching in the turbulent region. Formation of the hairpin vortex can lead to instability of the wake and cavity shedding dynamics as well as increasing the noise and pressure fluctuations.

To investigate effects of cavitating flow on the acoustic behavior, we applied the acoustic model of Ffowcs Williams–Hawkings [11]. This model used monitoring pressure fluctuation to transfer to the noise signal by considering monopole, dipole and quadrupole sources. In this analysis, the reference pressure of 10^{-6} Pa is applied, as recommended by Simanto et al. [2,8]. As shown in Fig. 7, the sound pressure level induced by low cavitation number ($\sigma = 2.57$) is significantly higher than that of non-cavitating condition ($\sigma = 4.95$) across the entire frequency ranges. This is attributed to the effects of the cavitating flow on the turbulent coherent structures, as reported in Fig. 6. As the cavity forms and collapses, it induces large-scaled turbulent structures. As a result, the monitoring point receives higher fluctuations of the pressure signal. This observation is consistent with experimental and numerical results reported by Simanto et al. [2,8].

Figure 8 compares the hydrodynamic characteristics under non-cavitating and cavitating flow conditions. In this analysis, the hydrodynamic coefficients are calculated using characteristic length of the chord length. As shown in the figure, formation of the cavity on the suction side of the hydrofoil induces significant variation in hydrodynamic behavior. In particular, under non-cavitating condition ($\sigma = 4.95$), the hydrodynamic signal is stable for both drag and lift features. However, as cavitating flow is considered ($\sigma = 2.57$), the hydrodynamic coefficients become unstable. This is due to formation and collapse of the cavity. As the cavity forms on the surface of the hydrofoil, it creates low pressure region. As the vapor collapses, it induces variation in the pressure distribution. As a consequence, this causes fluctuation of the hydrodynamic forces. Figure 9 shows pressure distribution on the suction side of the hydrofoil. This confirms the variation in the pressure behavior under cavitating conditions. The pressure is relatively uniform under non-cavitating conditions. As the cavitation number decreases and cavitating flow develops, the pressure becomes non-uniform, resulting in a stronger pressure gradient.

Figure 10 presents time-averaged volume fraction of vapor on the mid plane. As shown in the figure, the distribution of vapor on the plane considered is significantly different under non-cavitating and cavitating flow conditions. In particular, under non-cavitating flow condition ($\sigma = 4.95$), zero volume fraction of vapor is observed, indicating that the local pressure is relatively higher than the vapor pressure. However, as the cavitation number decreases to 2.57, approximately 50% volume fraction of vapor is clearly observed in the leading-edge region of the hydrofoil. The area of the vapor remains at 40% of the chord length. This result obviously confirms that decreasing cavitation number induces formation of the cavity on the suction side of the hydrofoil.

Figure 11 compares time-averaged flow streamlines around the hydrofoil. The streamlines are colored by streamwise velocity to show how it varies in non-cavitating and cavitating conditions. As shown in the figure, under high cavitation number, the streamlines are smooth, indicating a stable flow around the hydrofoil. However, as cavitating flow is considered (at lower cavitation number), the streamlines are significantly changed. In addition, a re-entrant jet is observed in the region of the cavitating flow. This illustrates the internal flow inside the cavitating flow. This entrant jet is physical mechanism for the cavity shedding and unstable flow.

4. CONCLUSION, LIMITATION AND FUTURE RESEARCH

This study numerically investigated the characteristics of cavitating flow around two-dimensional hydrofoil under both non-cavitating and cavitating flow conditions. The study applied LES, the Schnerr–Sauer cavitation model and Ffowcs Williams–Hawkings acoustic model to capture effects of cavitating flow on the flow behavior. The results showed that cavitating flow had significant effects on the velocity distribution, flow streamlines, pressure behavior, noise feature and hydrodynamic forces. This study confirmed that decreasing cavitation number induces formation of cavity on the suction side of the hydrofoil and hairpin vortex structures as the cavity collapses.

Although this study provides key findings of the cavitating flow, this remains several limitations such as scale effects and numerical errors due to cavitation turbulent models. In addition, experiment is required to quantitatively validate the numerical schemes. Future works should be carried out by both experimental and numerical methods to investigate the scale effects on the cavitating flow.

REFERENCES

[1] B. K. Ahn et al., “An experimental investigation of coherent structures and induced noise characteristics of the partial cavitating flow on a two-dimensional hydrofoil,” *Fluids*, vol. 5, no. 198, pp. 5040198, 2020.

[2] R. I. A. Simanto et al., “Experimental investigation on

cavitation and induced noise of two-dimensional hydrofoils with leading-edge protuberances," *Physics of Fluids*, vol. 34, no. 12, pp. 124115, 2022.
[3] **E.** Kadivar et al., "Control of unsteady partial cavitation and cloud cavitation in marine engineering and hydraulic systems," *Physics of Fluids*, vol. 32, no. 5, pp. 052108, 2020.
[4] L. Zhang, M. Chen, and X. Shao, "Inhibition of cloud cavitation on a flat hydrofoil through the placement of an obstacle," *Ocean Engineering*, vol. 155, no. 1, pp. 1-9, 2018.
[5] N. Heo and J. H. Kim, "Periodic behavior and noise characteristics of cavitation flow around two-dimensional hydrofoils," *Journal of Marine Science and Engineering*, vol. 12, no. 9, 2024.
[6] Z. Li et al., "Numerical simulation of the sheet/cloud cavitation around a two-dimensional hydrofoil using a modified URANS approach," *Journal of Mechanical Science and Technology*, vol. 31, no. 1, pp. 215-224, 2017.
[7] R. I. A. Simanto et al., "Comparative investigation of cavitating and non-cavitating flows around a two-dimensional hydrofoil using particle image velocimetry," *Physics of Fluids*, vol. 37, no. 1, pp. 017168, 2025.
[8] R. I. A Simanto et al., "Effects of leading-edge protuberances on cavitation induced noise and hydrodynamic performances of three-dimensional hydrofoils," *Journal of Fluid Mechanics*, vol. 1016, no. A56, 2025.
[9] V. D. Pham and B. K Ahn, "Large eddy simulation investigation on the effects of the forebody shape of a supercavitating torpedo," *Physics of Fluids*, vol. 36, no. 10, pp. 103343, 2024.
[10] P. J. Roache, "Perspective: A method for uniform reporting of grid refinement studies," *Journal of Fluids Engineering*, vol. 116, no. 3, pp. 405-413, 1994.
[11] J. E. F. Williams and D. L. Hawkings, "Theory relating to the noise of rotating machinery," *Journal of Sound Vibration*, vol. 10, no. 1, pp. 10-21, 1969.
[12] H. K. Versteeg and W. Malalasekera, *An introduction to computational fluid dynamics: The finite volume method*, Pearson Education Limited, 2007.
[13] G. H. Schnerr and J. Sauer, "Physical and numerical modeling of unsteady cavitation dynamics," *Proc. of 4th International conference on multiphase flow*, New Orleans, USA, 2001.